R.E.M. (Rekayasa Energi Manufaktur) Jurnal | Vol.11 No.2/2026
ISSN online (2528-3723)
http://doi.org/10.21070/rem.v11i2.1862

Erosion Behavior of Cr_3C_2-NiCr Coated GH4720Li Superalloy Under Different Impact Angles and Erodent Sizes: A Finite Element Analysis

Raffi Indrajati[1], Riki Hendra Purba[1*], James Julian[1], Fitri Wahyuni[1],
Elvi Armadani[2], Fathin Muhammad Mardhudhu[3], Kenta Kusumoto[4]
[*]Email corresponding author: Rikihendrapurba@upnvj.ac.id

[1]*Department of Mechanical Engineering, Universitas Pembangunan Nasional Veteran Jakarta, 12450, Indonesia*
[2]*Department of Industrial Engineering, Universitas Pembangunan Nasional Veteran Jakarta, 12450, Indonesia*
[3]*Department of Naval Architecture, Universitas Pembangunan Nasional Veteran Jakarta, 12450, Indonesia*
[4]*College of Design and Manufacturing Technology, Muroran Institute of Technology, Japan*

Article history: Received: 30 Juni 2026 | Revised: 22 Juli 2026 | Accepted: 27 Juli 2026

Abstract. *Solid particle erosion is a critical issue for turbine blade materials operating in harsh environments. This study investigates the erosion behavior of Cr_3C_2-NiCr coated GH4720Li superalloy using a three-dimensional single-particle finite element model. Silica sand particles with diameters of 0.3, 0.5, and 0.7 mm impacted the surface at 30°, 60°, and 90°, while material behavior was described by the strain-rate-dependent Cowper–Symonds model. The results show that both impact angle and particle size significantly affect stress distribution, plastic deformation, and erosion behavior. Higher impact angles and larger particles produce greater von Mises stress and effective plastic strain, with maximum values at 90° and 0.7 mm. The erosion mechanism changes from cutting at 30° to combined cutting and crater formation at 60°, and localized crater formation at 90°. The Cr_3C_2-NiCr coating improves erosion resistance by reducing stress concentration and plastic deformation through impact energy absorption and redistribution.*

Keywords - *Solid particle erosion; Cr_3C_2-NiCr coating; GH4720Li superalloy; Finite element analysis; Impact anglse; Particles sizes*

INTRODUCTION

Damage caused by erosion is common in the oil and gas, aviation and mining industries [1], [2], [3]. This damage can lead to the degradation of material surfaces, which may reduce the service life of equipment and increase maintenance costs, particularly in the case of turbine blades, which are prone to solid particle erosion [4]. Erosion, and solid particle erosion in particular, is a phenomenon in which material degrades as a result of repeated impacts from particles carried by a fluid [5], [6], [7].

Materials with high yield strength and fatigue resistance are often used in turbine blades, such as GH4720Li [8]. Turbine blades are crucial components of aero-engines and operate in erosive environments. Consequently, the erosion resistance of these materials affects the performance and reliability of the engines [9], [10].

With the rapid advancement of technology, coating technologies have emerged as an effective approach for mitigating erosion on material surfaces. Among these, cermet coatings have attracted considerable attention due to their excellent resistance to wear and oxidation, making them suitable for demanding engineering applications. Previous studies have demonstrated that Cr_3C_2-based coatings deposited through thermal spray techniques exhibit significant potential for protecting engineering components operating in erosive environments by enhancing their surface durability and extending their service life [11], [12].

Using silica sand particles with a diameter of 700 µm, Yaer et al. (2019) [8] investigated the erosion behavior of three superalloys, namely GH4720Li, GH738, and GH4169, under impact angles ranging from 30° to 90° and particle velocities of 25 and 55 m/s. Their numerical predictions showed good agreement with the experimental results, demonstrating the reliability of the finite element approach for erosion analysis. Similarly, Zhang and Dong (2015) [13] employed Finite Element Analysis (FEA) to evaluate the erosion resistance of cermet-coated superalloy substrates subjected to repeated solid particle impacts. Considering the effects of coating thickness, particle velocity, and particle size, they reported that coatings thicker than 100 µm significantly enhanced erosion resistance, while the developed model accurately predicted erosion damage consistent with experimental observations. Furthermore, Zhang et al. (2017) [14] used a three-dimensional FEA model to investigate the influence of impact angle, particle velocity, particle size, and material properties on the erosion behavior of Q345 steel. Their results revealed that particle velocity and particle size are dominant parameters governing erosion wear, with higher particle velocities leading to increased erosion rates. These findings are consistent with the earlier work of Bahadur and Badruddin (1990) [15], who demonstrated that particle size and particle shape play critical roles in determining both the erosion mechanisms and the resulting erosion rate. In previous research [16], it has been investigated the effect of impact velocity on GH4720Li material with a Cr_3C_2 coating using finite element analysis. The results showed that higher velocities result in greater maximum stress due to the increased kinetic energy carried by the eroding particles. However, the influence of impact particle size under diffrent was not chomprehensively exproled.

Therefore, this study investigates the erosive wear behavior of Cr_3C_2–NiCr-coated GH4720Li under different impact angles of 30°, 60°, and 90°. In addition, three particle sizes, namely 0.3 mm, 0.5 mm, and 0.7 mm, are considered in the analysis. The combined effects of these impact angles and particle sizes on this coating–substrate system have not been comprehensively investigated in previous studies. The analysis focuses on key dynamic parameters, including stress distribution, plastic deformation, and surface damage characteristics.

METHODS

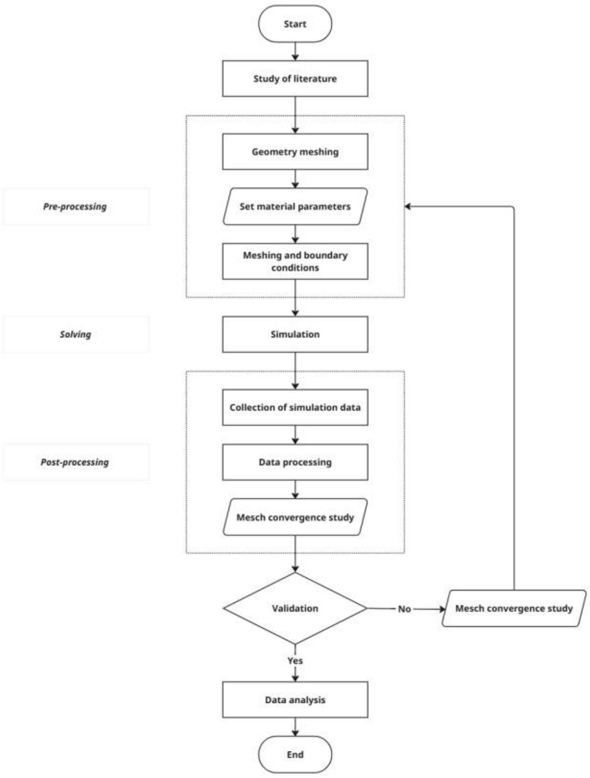

Figure 1. Research flowchart

In this study, the research and simulation workflow is organized into several sequential stages, as illustrated in Figure 1. The process begins with a comprehensive literature review to establish the scientific foundation of the study by examining previous research and relevant theoretical concepts. Subsequently, the pre-processing stage is conducted, including geometry creation, mesh generation, definition of boundary conditions, and assignment of material properties required for the finite element model.

Following the completion of the pre-processing stage, the simulation is performed using the Finite Element Analysis (FEA) method. The resulting data are then extracted and evaluated during the post-processing stage. A mesh convergence study is conducted to verify the numerical accuracy and independence of the computational model. The simulation results are subsequently validated by comparison with available experimental data or published numerical results. If the validation criteria are not satisfied, the model is refined by revisiting the pre-processing stage, and the simulation is repeated until acceptable agreement is achieved. Finally, the validated results are comprehensively analyzed to evaluate the erosion behavior, providing a systematic and reliable workflow from model development to the interpretation of the simulation outcomes.

A. Material

In this study, the Cowper-Symonds strain rate dependent constitutive model is employed to describe the material behavior under dynamic loading conditions. The Cr_3C_2-NiCr coated GH4720Li superalloy is modeled as the target material, while silica sand (SiO_2) particles are used as the erodent in the numerical simulations. The yield stress (σ_y) and the plastic hardening modulus (E_p) required for the Cowper–Symonds model are calculated using Equations (1) and (2), respectively [17].

$$\sigma_y = [1 + (\varepsilon/\dot{C})^{\frac{1}{P}}](\sigma_0 + \beta E_p \varepsilon_P^{eff}) \quad (1)$$

$$E_P = \frac{E_{tan} E}{E - E_{tan}} \quad (2)$$

Table 1. Material Properties [18], [19], [20], [21], [22], [23], [24]

Materials	Density (kg/mm^3)	Poisson's Ratio	Young's Modulus (GPa)
Cr_3C_2-NiCr	6.7 x 10^{-6}	0.25	280
GH4720Li	8.2 x 10^{-6}	0.30	220
SiO_2	2.65 x 10^{-6}	0.19	74.8

B. Simulation Geometry

A three-dimensional Finite Element Analysis (FEA) model was developed using ls dyne engineering software to investigate the erosion behavior of Cr_3C_2-NiCr-coated GH4720Li under three different impact angles and three different particles sizes with 75 m/s impact velocity. Silica sand (SiO_2) particles with a diameter of 0.7 mm were selected as the erodent based on the experimental conditions reported by Yaer et al. [8] and further developed into 0.3, 0.5 and 0.7 mm. The target specimen was modeled with dimensions of 1 × 1 × 0.6 mm and a coating thickness of 0.1 mm. The impact angles considered in the simulations were 30°, 60°, and 90°. The numerical model employed a hexahedral mesh for both the target materials (coating and substrate) and the impacting particles. The simulation was performed with a termination time of 0.0075 ms and a time step of 0.00015 ms. The geometry and boundary condition of the numerical model is presented in Figure 2.

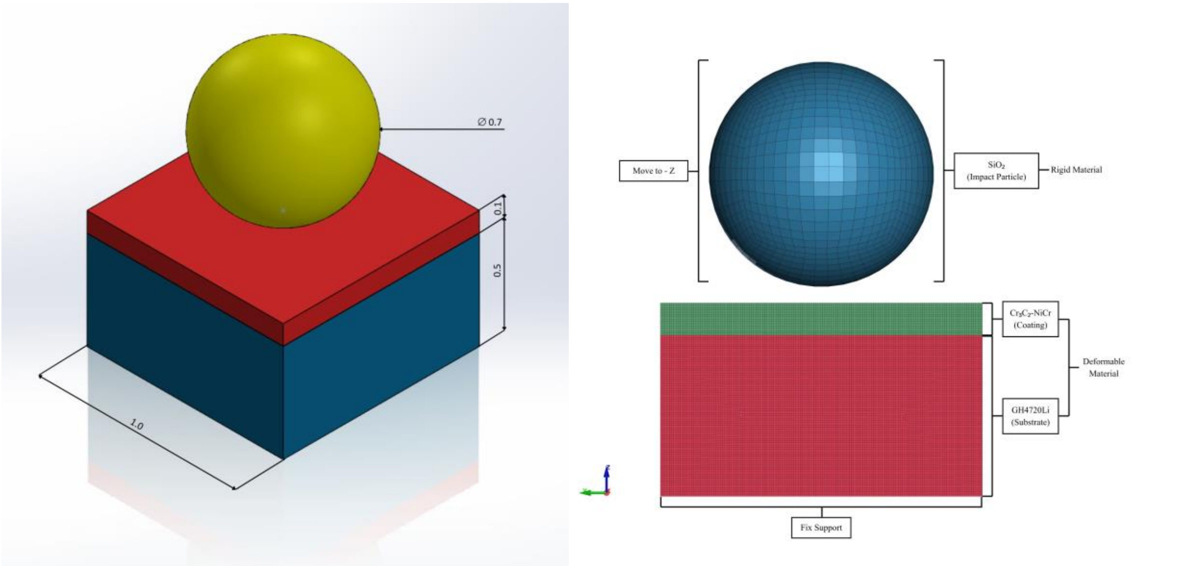

Figure 2. Simulation geometry and boundary condition

C. Mesh Convergence Study

A mesh convergence study was conducted to ensure that the numerical results were independent of mesh discretization and to verify the accuracy of the finite element model [25], [26]. Five mesh densities were evaluated, consisting of 62,500, 256,000, 500,000, 1.0 × 10^6, and 1.5 × 10^6 elements. Mesh convergence was assessed by comparing the maximum von Mises stress in the target material. As the mesh density increased, the variation in the predicted maximum stress gradually decreased, indicating improved numerical convergence and solution stability. A mesh containing 1.0 × 10^6 elements was therefore selected for all subsequent simulations, as it produced a maximum stress variation of only 0.73% while substantially reducing the computational cost relative to the finest mesh.

Table 2. Mesh convergence study

Mesh Density	Maximum Stress (GPa)	Error (%)
62500	1.1183710098	
2560	1.2531775236	10.76
500000	1.2954077721	3.26
10^6	1.3098628521	1.1
1.5×10^6	1.3194630146	0.73

RESULT AND DISCUSSION

A. Validation

To verify the reliability of the numerical model, a validation study was conducted by comparing the simulation results with the published data reported by Yaer et al. [8]. The validation model employed GH4720Li as the target material subjected to a particle impact velocity of 25 m/s at a normal impact angle of 90°. The effective stress distributions beneath the target surface were evaluated along the x, y, and z directions. As shown in Figure 3, the predicted stress profiles exhibit good agreement with the reference results, demonstrating the capability of the proposed finite element model to accurately capture the stress response induced by particle impact. Minor discrepancies were observed in the region located approximately 25 - 80 µm beneath the impacted surface. These deviations are attributed to differences in the adopted material properties, constitutive parameters, and numerical modeling assumptions between the present study and the reference model.

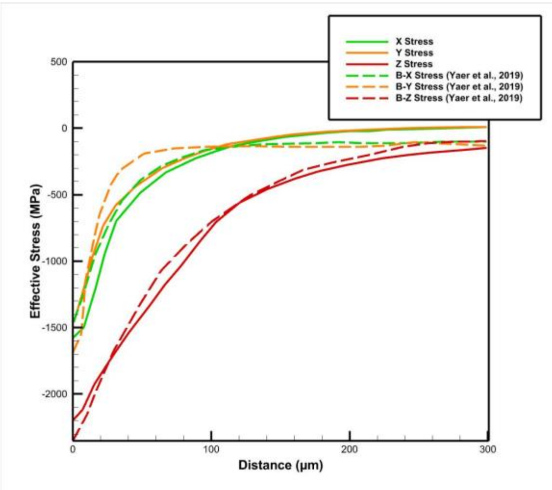

Figure 3. Simulation validation result

B. Effective Stress (von-Mises)

Xiao et al. (2017) [24] defined von Mises stress as a function of the three principal stresses and demonstrated its effectiveness as a criterion for evaluating the mechanical response of iron-based and steel materials under impact loading. Figure 5 illustrates the distribution of von Mises stress in both coated and uncoated GH4720Li at different impact angles and different particles sizes. The research results show a consistent trend, whereby the maximum von Mises stress increases as the impact angle increases, regardless of the presence or absence of a Cr_3C_2-NiCr coating. This behavior is attributed to the larger normal component of the impact force at higher impact angles, which produces greater localized compressive and equivalent stresses beneath the impact site. Consequently, the higher stress concentration promotes more severe surface damage and contributes to an increased erosion rate, which generally reaches its maximum value at or near a normal impact angle of 90° [25]. The highest effective stress was observed in the uncoated material subjected to particle impact at an angle of 90°. The effective stress reached 6.8 GPa, 6.9 GPa, and 6.5 GPa for particle sizes of 0.7 mm, 0.5 mm, and 0.3 mm, respectively. In contrast, the Cr_3C_2-NiCr coated material exhibited significantly lower effective stress values under the same impact conditions, with stresses of 3.7 GPa, 2.0 GPa, and 1.4 GPa for particle sizes of 0.7 mm, 0.5 mm, and 0.3 mm, respectively. These results demonstrate that the coating effectively reduces the stress generated during particle impact, thereby mitigating stress concentration and improving the material's resistance to erosive loading.

The highest stress concentration occurs beneath the contact area (surface); this is consistent with Hertzian Contact theorem [27], as can be seen in the Figure 4(d)(e)(f). The Figure 4(f) illustrates the von Mises stress distribution at an impact angle of 30°, where the stress concentration is primarily localized along the particle trajectory. At an impact angle of 60° Figure 4(e), the stress distribution remains aligned with the particle motion but extends over a wider region due to the increased normal component of the impact force. In contrast, the stress contours at a normal impact angle of 90° Figure 4(d) exhibit a broader and more symmetric distribution beneath the impact site. These observations indicate that increasing the impact angle promotes a wider and more uniform distribution of stress within the target material. Furthermore, the Cr_3C_2-NiCr coating consistently reduces the stress transmitted to the GH4720Li substrate at all impact angles, as shown in Figure 4. This behavior demonstrates that the coating effectively absorbs and redistributes part of the impact energy, thereby lowering the stress concentration within the substrate. As a result, the likelihood of plastic deformation, crack initiation, and premature substrate failure is significantly reduced.

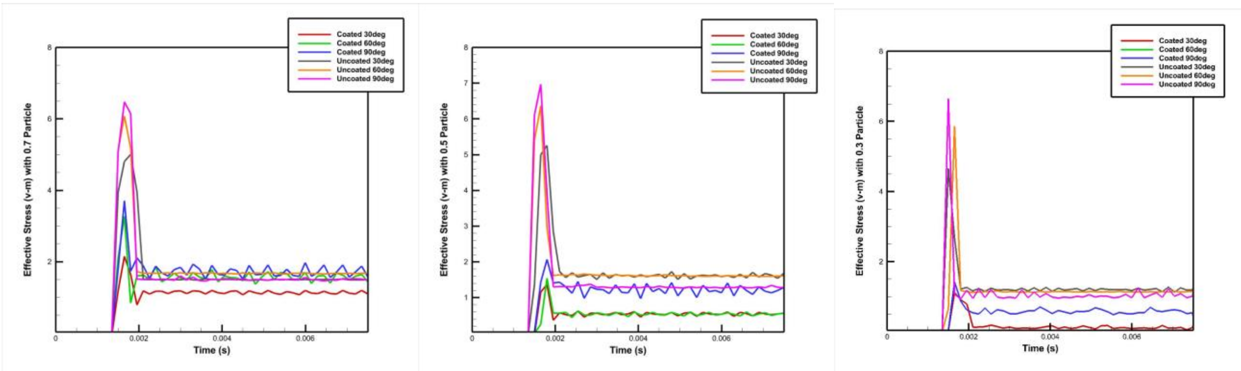

(a) Particle 0.7mm (b) Particle 0.5mm (c) Particle 0.3mm

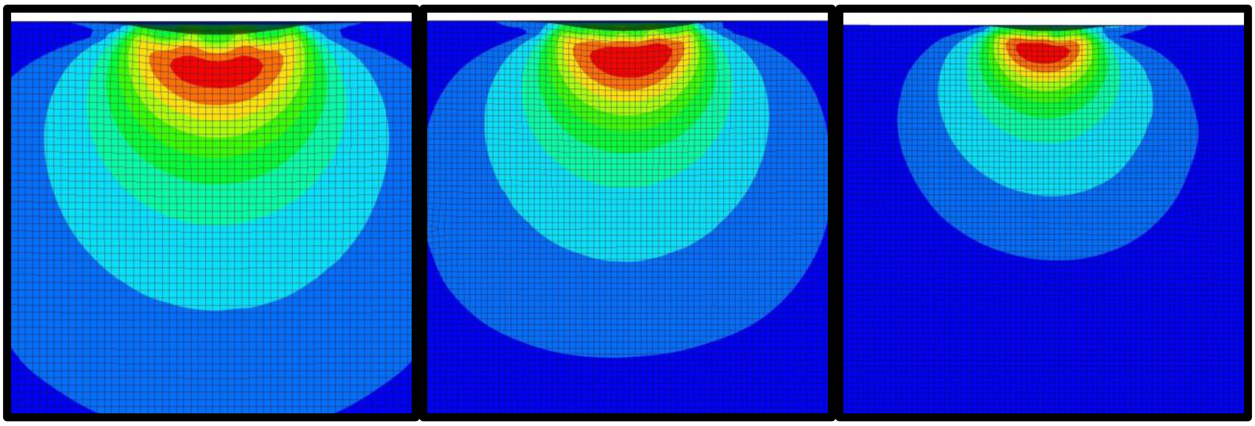

(d) Stress Contour at 90deg (e) Stress Contour at 60deg (f) Stress Contour at 30deg

Figure 4. Maximum Effective Stress

C. Effective Plastic Strain

The Cr_3C_2-NiCr coating significantly reduces the maximum effective plastic strain developed in the GH4720Li substrate across all particle sizes and impact angles. For instance, under a 90° impact angle with a particle size of 0.7 mm, the maximum effective plastic strain in the uncoated substrate reached 0.078 GPa, whereas the coated substrate exhibited a substantially lower value of 0.043 GPa. This reduction demonstrates the coating's ability to absorb and redistribute the impact energy, thereby mitigating plastic deformation and enhancing the erosion resistance of the substrate. This behavior indicates that the coating absorbs and redistributes a portion of the impact energy before it is transmitted to the substrate, thereby mitigating localized plastic deformation. In contrast, the uncoated substrate is directly exposed to the impact load, resulting in more severe plastic deformation, particularly at higher impact angles approaching 90°, where the normal component of the impact force is dominant [28].

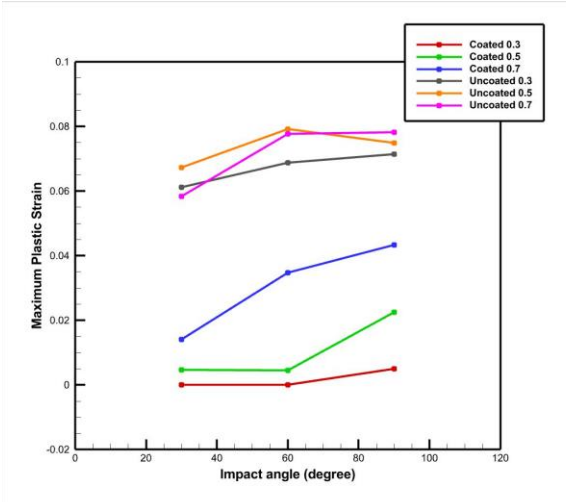

Figure 5. Maximum Plastic Strain

D. Surface Deformation of the Model

Figure 6 illustrates the surface deformation of the material induced by particle impact at different impact angles. At an impact angle of 30°, the predominant deformation feature is the formation of lips on the surface, indicating the occurrence of micro-cutting and micro-ploughing wear mechanisms. This behavior results from the oblique interaction between the erodent particle and the target surface, where the particle trajectory is deflected after impact. Consequently, the displaced material flows in the direction of particle motion, producing characteristic lip formations around the impact region [29]. As the impact angle increases to 60°, the deformation pattern changes significantly. Both craters and lips are observed simultaneously, suggesting the coexistence of micro-cracking, micro-cutting, and micro-ploughing wear mechanisms. This combination of deformation features indicates a transition in the dominant erosion mechanism at the intermediate impact angle, as shown in Figure 6 [29], [30]. At an impact angle of 90°, the erodent particles strike the target surface almost perpendicularly, with little or no deflection of their trajectories. Under these conditions, the particle kinetic energy is concentrated within a smaller contact area, resulting in the formation of deeper and more pronounced craters compared with those produced at lower impact angles. The dominant wear mechanism in this case is micro-cracking, which is associated with severe localized material damage [31]. Consequently, the Cr_3C_2–NiCr cermet coating experiences the highest degree of localized deformation under normal impact conditions, reflecting the greater intensity of impact loading and stress concentration.

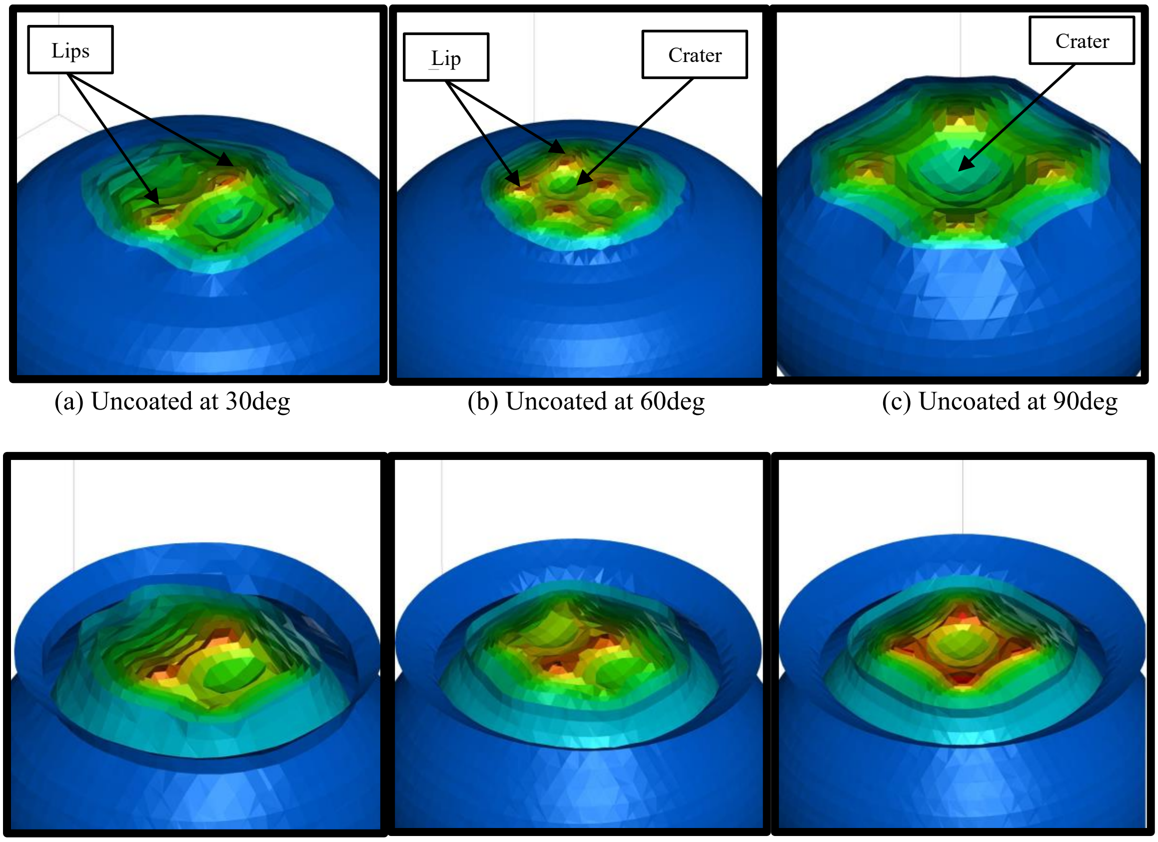

(a) Uncoated at 30deg (b) Uncoated at 60deg (c) Uncoated at 90deg

(d) Coated at 30deg (e) Coated at 60deg (f) Coated at 90deg

Figure 6. Surface Deformation

Conclusion

This study investigated the mechanical response and erosion behavior of Cr_3C_2-NiCr coated and uncoated GH4720Li under solid particle impact using a three-dimensional single-particle finite element model at various impact angles and particle sizes. The results indicate that the impact angle has a significant influence on stress distribution, plastic deformation, and surface damage. The maximum von Mises stress consistently increases with increasing impact angle, reaching its highest value at normal impact (90°) due to the dominance of the normal component of the impact force. The stress concentration is primarily localized beneath the contact area, in accordance with Hertzian contact theory, and becomes broader and more symmetric as the impact angle increases.

The Cr_3C_2-NiCr coating effectively reduces both the maximum von Mises stress and effective plastic strain transmitted to the GH4720Li substrate across all investigated conditions. By absorbing and redistributing a portion of the impact energy, the coating mitigates stress concentration, suppresses localized plastic deformation, and lowers the likelihood of crack initiation and substrate failure. Surface deformation analysis further reveals a transition in the dominant erosion mechanism with increasing impact angle. At 30°, erosion is characterized mainly by micro-cutting and micro-ploughing accompanied by lip formation. At 60°, crater formation and lip development coexist, indicating the combined action of micro-cutting, micro-ploughing, and micro-cracking. Under normal impact (90°), deeper crater formation and severe localized damage become dominant as micro-cracking emerges as the primary wear mechanism.

From an engineering application, these findings demonstrate the potential of Cr_3C_2–NiCr coatings to improve the durability and operational reliability of turbine blades exposed to solid particle erosion in gas turbine environments. Turbine blades frequently encounter airborne particles such as dust, sand, ash, and combustion by-products, which can impact blade surfaces at various angles and induce severe stress concentrations and material degradation. The ability of the Cr_3C_2–NiCr coating to reduce impact-induced stresses and plastic deformation suggests that it can effectively delay erosion-induced damage, preserve blade aerodynamic profiles, and minimize the risk of crack initiation during long-term service. Consequently, the application of Cr_3C_2–NiCr coatings on GH4720Li turbine blades can contribute to extended component service life, reduced maintenance frequency, improved turbine efficiency, and enhanced operational safety, particularly in harsh environments where particle erosion is a critical failure mechanism.

REFERENCE

[1] R. Tarodiya and A. Levy, "Surface erosion due to particle-surface interactions - A review," Jul. 01, 2021, *Elsevier B.V.* doi: 10.1016/j.powtec.2021.04.055.

[2] R. J. K. Wood, "The sand erosion performance of coatings," 1999.

[3] R. J. K. Wood, B. G. Mellor, and M. L. Binfield, "WEAR Sand erosion performance of detonation gun applied tungsten carbide/cobalt-cbxomium coatings," 1997.

[4] T. Deng, "Erosive Wear Mechanisms of Materials—A Review of Understanding and Progresses," Apr. 01, 2025, *Multidisciplinary Digital Publishing Institute (MDPI)*. doi: 10.3390/ma18071615.

[5] I. Finnie, "Erosion of surfaces by solid particles," *Wear*, vol. 3, no. 2, pp. 87–103, 1960, doi: https://doi.org/10.1016/0043-1648(60)90055-7.

[6] K. Shimizu *et al.*, "Microstructural evaluation and high-temperature erosion characteristics of high chromium cast irons," *Wear*, vol. 426–427, pp. 420–427, 2019, doi: https://doi.org/10.1016/j.wear.2019.01.043.

[7] A. Hamed, W. Tabakoff, and R. Wenglarz, "Erosion and deposition in turbomachinery," 2006, *American Institute of Aeronautics and Astronautics Inc.* doi: 10.2514/1.18462.

[8] X. Yaer *et al.*, "Surface deformation micromechanics of erosion damage at different angles and velocities for aero-engine hot-end components," *Wear*, vol. 426–427, pp. 527–538, Apr. 2019, doi: 10.1016/j.wear.2018.12.054.

[9] A. J. Freimanis, A. E. Segall, J. C. Conway Jr, and E. J. Whitney, "The influence of temperature on the wear mode and deterioration of coatings used for titanium aircraft engine components," *Tribology transactions*, vol. 45, no. 2, pp. 193–198, 2002.

[10] B. M. Silayev and P. A. Danilenko, "Method of calculating high-speed rolling bearings intended for an aircraft engine based on considering the wear process," *Journal of Friction and Wear*, vol. 36, no. 4, pp. 350–354, 2015.

[11] S. Mahade, A. Mulone, S. Björklund, U. Klement, and S. Joshi, "Novel suspension route to incorporate graphene nano-platelets in HVAF-sprayed Cr3C2–NiCr coatings for superior wear performance," *Journal of Materials Research and Technology*, vol. 13, pp. 498–512, Jul. 2021, doi: 10.1016/j.jmrt.2021.04.096.

[12] A. Rajabi, M. J. Ghazali, and A. R. Daud, "Chemical composition, microstructure and sintering temperature modifications on mechanical properties of TiC-based cermet - A review," Feb. 15, 2015, *Elsevier Ltd*. doi: 10.1016/j.matdes.2014.10.081.

[13] H. Zhang and X. Dong, "Finite element analysis of multiple solid particles erosion in cermet coating," *Surf. Coat. Technol.*, vol. 262, pp. 184–190, Jan. 2015, doi: 10.1016/j.surfcoat.2014.12.040.

[14] C. Zheng, Y. Liu, C. Chen, J. Qin, and S. Zhang, "Finite element analysis on the dynamic erosion process using multiple-particle impact model," *Powder Technol.*, vol. 315, pp. 163–170, 2017, doi: https://doi.org/10.1016/j.powtec.2017.04.016.

[15] S. Bahadur and R. Badruddin, "Erodent particle characterization and the effect of particle size and shape on erosion," *Wear*, vol. 138, no. 1, pp. 189–208, 1990, doi: https://doi.org/10.1016/0043-1648(90)90176-B.

[16] R. H. Purba, Raffi Indrajati, Fitri Wahyuni, James Julian, Elvi Armadani, and Fathin Muhammad Mahdhudhu, "Finite Element Analysis of Impact-Velocity Effects on the Erosion Behavior of GH4720Li Superalloy-Based Cr_3C_2 Coatings," *Jurnal Asiimetrik: Jurnal Ilmiah Rekayasa & Inovasi*, pp. 111–122, Jan. 2026, doi: 10.35814/asiimetrik.v8i1.9317.

[17] C. Hernandez, A. Maranon, I. A. Ashcroft, and J. P. Casas-Rodriguez, "A computational determination of the Cowper-Symonds parameters from a single Taylor test," *Appl. Math. Model.*, vol. 37, no. 7, pp. 4698–4708, Apr. 2013, doi: 10.1016/j.apm.2012.10.010.

[18] P. E. Aba-Perea, T. Pirling, P. J. Withers, J. Kelleher, S. Kabra, and M. Preuss, "Determination of the high temperature elastic properties and diffraction elastic constants of Ni-base superalloys," *Mater. Des.*, vol. 89, pp. 856–863, Jan. 2016, doi: 10.1016/j.matdes.2015.09.152.

[19] P. E. Aba-Perea, P. J. Withers, T. Pirling, A. Paradowska, D. Ma, and M. Preuss, "In Situ Study of the Stress Relaxation During Aging of Nickel-Base Superalloy Forgings," *Metall. Mater. Trans. A Phys. Metall. Mater. Sci.*, vol. 50, no. 8, pp. 3555–3565, Aug. 2019, doi: 10.1007/s11661-019-05302-0.

[20] D. He, F. Mao, X. Pan, L. Shang, and X. Li, "Optimizing high-temperature tribological properties of Cr3C2-NiCr/AlCrN duplex coatings by adjusting Cr3C2 contents," *Ceram. Int.*, 2025, doi: 10.1016/j.ceramint.2025.05.241.

[21] L. Janka, *Thermally Sprayed Cr 3 C 2-NiCr Coatings-Improving the Abrasion Resistance*. 2018.

[22] E. Jonda, L. Łatka, and W. Pakieła, "Microstructure and selected properties of cr3c2–nicr coatings obtained by hvof on magnesium alloy substrates," *Materials*, vol. 13, no. 12, pp. 1–12, Jun. 2020, doi: 10.3390/ma13122775.

[23] N. Sharma, T. Saxena, S. N. Alam, B. C. Ray, K. Biswas, and S. K. Jha, “Ceramic-based nanocomposites: A perspective from carbonaceous nanofillers,” Jun. 01, 2022, *Elsevier Ltd*. doi: 10.1016/j.mtcomm.2022.103764.

[24] J. Kang *et al.*, “Advanced composite material: effect of composite SiC on compressive strength and hardness of porous titanium,” *Journal of Materials Research and Technology*, vol. 16, pp. 960–967, Jan. 2022, doi: 10.1016/j.jmrt.2021.12.037.

[25] H. Patil and P. V. Jeyakarthikeyan, “Mesh convergence study and estimation of discretization error of hub in clutch disc with integration of ANSYS,” in *IOP Conference Series: Materials Science and Engineering*, Institute of Physics Publishing, 2018. doi: 10.1088/1757-899X/402/1/012065.

[26] J. Julian, W. Iskandar, F. Wahyuni, and F. Ferdyanto, “COMPUTATIONAL FLUID DYNAMICS ANALYSIS BASED ON THE FLUID FLOW SEPARATION POINT ON THE UPPER SIDE OF THE NACA 0015 AIRFOIL WITH THE COEFFICIENT OF FRICTION,” *Media Mesin: Majalah Teknik Mesin*, vol. 23, pp. 70–82, Jan. 2022, doi: 10.23917/mesin.v23i2.18217.

[27] B. Mitchell, Y. Yokoyama, A. Nassiri, Y. Tagawa, Y. P. Korkolis, and B. L. Kinsey, “An investigation of Hertzian contact in soft materials using photoelastic tomography,” *J. Mech. Phys. Solids*, vol. 171, p. 105164, 2023, doi: https://doi.org/10.1016/j.jmps.2022.105164.

[28] K. L. Johnson, “One Hundred Years of Hertz Contact,” *Proceedings of the Institution of Mechanical Engineers*, vol. 196, no. 1, pp. 363–378, 1982, doi: 10.1243/PIME_PROC_1982_196_039_02.

[29] R. H. Purba *et al.*, “Erosive wear characteristics of high-chromium based multi-component white cast irons,” *Tribol. Int.*, vol. 159, p. 106982, 2021, doi: https://doi.org/10.1016/j.triboint.2021.106982.

[30] Y. Gaqi, K. Kusumoto, K. Shimizu, and R. H. Purba, “Effect of Carbide Orientation on Wear Characteristics of High-Alloy Wear-Resistant Cast Irons,” *Lubricants*, vol. 11, no. 7, 2023, doi: 10.3390/lubricants11070272.

[31] K. Kusumoto, K. Shimizu, R. H. Purba, and Y. Momma, “Effect of carbide refinement on high temperature erosive wear behavior of high chromium white cast iron with different titanium and carbon additions,” *Mater. Today Commun.*, vol. 39, p. 109276, 2024, doi: https://doi.org/10.1016/j.mtcomm.2024.109276.

This page is intentionally left blank